Tight-binding study of the lattice dynamics of graphite

K. C. Hass
Ford Motor Company, Research Staff, SRL/MD S-3028, Dearborn, Michigan 48121-2053
(Received 14 November 1991)

The vibrational spectrum of a two-dimensional (2D) sheet of graphite is examined using a tight-binding total-energy formalism. Motivation for this work is provided by the poor transferability of classical valence-force models for sp^2 carbon. A major problem with such models is the neglect of π-electron polarizability. The full tight-binding formalism considered here includes both this effect and covalent σ bonding on the same footing. Atomic force constants of arbitrary range are calculated quantum mechanically using a Green's-function approach. Long-range interactions, resulting from delocalized π bonding, are shown to be important for in-plane vibrations. The restoring forces for out-of-plane vibrations are dominated by σ-π mixing. The resulting phonon spectrum for 2D graphite is accurate only to within 30%. This is considerably worse than previous tight-binding results for sp^3 solids. Some possible reasons for this are discussed. The difficulties encountered here may well impede our ability to understand the vibrational properties of more complicated π-bonded solids, particularly amorphous carbons and fullerenes.

I. INTRODUCTION

It is well known among quantum chemists that delocalized π bonding may give rise to long-range interactions that contribute significantly to vibrational properties.[1] This effect appears to have been appreciated only recently by condensed matter physicists in the context of conducting polymers.[2–5] Some methods for calculating the vibrational spectra of solids (e.g., "frozen-phonon" calculations within density-functional theory[6]) include this effect automatically. Most simpler methods (e.g., valence force calculations[7,8]) do not. A poor understanding of this point may be in part responsible for the limited accuracy of many early vibrational calculations for fullerenes.[9] The present work was stimulated more directly by the rich, but largely unexplained, Raman spectra of amorphous carbons.[10,11] Both fullerenes and amorphous carbons are composed entirely, or predominantly, of threefold coordinated, sp^2 (or nearly sp^2), π-bonded carbon. The present work focuses on the prototypical π-bonded solid, graphite, which is also composed of sp^2 carbon. Surprisingly, in all of the enormous literature on the lattice dynamics of graphite,[12] there does not appear to be any explicit mention of the role of delocalized π bonding.

For the present study, it suffices to consider a single two-dimensional (2D) graphitic layer. The weak interlayer interactions in crystalline graphite have minor effects on the vibrational spectrum[12] and are thus reasonably ignored for simplicity. The theoretical approach used here is that of tight-binding total-energy theory.[13] This is the simplest method available for calculating phonon spectra that is fully quantum mechanical; its description of delocalized π bonding is similar to that of the well-known Hückel molecular orbital theory of quantum chemistry.[1] Tight-binding phonon calculations have been performed previously both for bulk crystals (mostly transition metals[14] and semiconductors[15]) and for crystalline surfaces.[16] Mazur and Pollmann[17] have recently given a detailed exposition of this approach for the case of crystalline Si. The present formalism closely follows that of Ref. 17 although it is convenient here to separate out the effects of σ and π bonding. For in-plane motions of the carbon atoms in 2D graphite, the contributions of σ (sp^2 orbital) and π (p orbital $\perp$ plane) electrons are completely separable by symmetry. For out-of-plane motions, the σ and π electrons mix; the restoring force to a planar structure is provided by the energy increase associated with this mixing.

Most previous studies of the lattice dynamics of graphite have been based on empirical force constant models.[12] The most successful of these is generally believed to be that of Al-Jishi and Dresselhaus[18] (AD), which includes up to fourth neighbor in-plane interactions. The AD model was fitted to an extensive data set composed of elastic constants, optical frequencies, and inelastic neutron-scattering results. The phonon dispersion curves calculated from this model for 2D graphite[19] are shown in Fig. 1 for reference. Also shown are the recent electron-energy-loss results of Oshima *et al.*[20,21] The curves along Γ-M are labeled as in Ref. 21: O and A denote optic and acoustic branches and L and Z refer to in-plane longitudinal and out-of-plane motion, respectively; SH denotes shear horizontal modes which are neither purely transverse nor purely longitudinal. The AD model provides a good overall fit to the data but is still deficient in some respects, e.g., the crossing of the LA and SH branches near 1250 cm^{-1}. The goal of the present work is not to improve on the AD model, but simply to explore the relationship between the vibrational spectrum in Fig. 1 and the electronic structure. An understanding of this relationship is crucial for the development of more transferable approaches that would provide reasonable results not just for graphite, but for all sp^2 carbon environments.

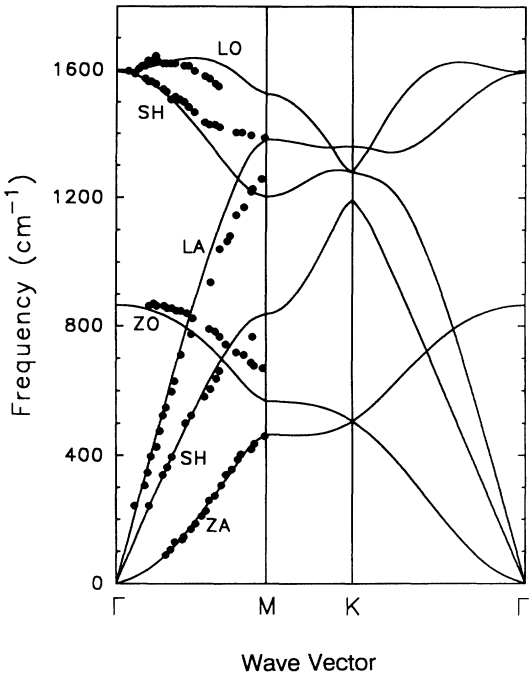

FIG. 1. Phonon dispersions curves for 2D graphite calculated using the model of Al-Jishi and Dresselhaus (Ref. 18). The dots are experimental data from Ref. 20. Γ, *M*, and *K* refer to the center, edge, and corner of the hexagonal Brillouin zone. The branch labels are described in the text.

II. VALENCE FORCE MODELS AND π-ELECTRON POLARIZABILITY

The Kirkwood[7] and Keating[8] valence force models for sp^2 carbon may be defined as

$$H_{\text{Kirk}}=\frac{k_r}{2}\sum_{\langle ij\rangle}(|\mathbf{x}_{ij}|-d_0)^2+\frac{k_\theta d_0^2}{2}\sum_{\langle ijk\rangle}(\theta_{ijk}-\theta_0)^2 \quad (1)$$

and

$$H_{\text{Keat}}=\frac{k_s}{8d_0^2}\sum_{\langle ijk\rangle}(\mathbf{x}_{ij}\cdot\mathbf{x}_{ij}-d_0^2)^2 + \frac{k_b}{2d_0^2}\sum_{\langle ijk\rangle}(\mathbf{x}_{ji}\cdot\mathbf{x}_{jk}-d_0^2\cos\theta_0)^2 , \quad (2)$$

where $\mathbf{x}_{ij}$ is the vector from site i to site j, θ_{ijk} is the angle subtended by sites i and k about site j, d_0 is the equilibrium bond length, and $\theta_0=120°$ is the equilibrium bond angle. The first sums in Eqs. (1) and (2) are over all nearest-neighbor bonds and the second sums are over all nearest-neighbor bond angles. In general, both of these models yield similar results. The Kirkwood model was employed by Beeman *et al.*[23] in their pioneering study of the vibrational properties of amorphous carbon networks. The Keating model gives slightly better results for 2D graphite, but will be seen below to be equally deficient in its transferability to benzene.

Figure 2 shows dispersion curves resulting from the Keating (solid) and Kirkwood (dashed) models for the

This desire for transferability, of course, lies at the heart of classical valence force methods. The so-called Kirkwood[7] and Keating[8] models (two-parameter bond-stretching and bond-bending models) work very well for sp^3-bonded solids,[22] but less well for sp^2 carbon. Section II of this paper illustrates this problem by considering the extreme cases of 2D graphite and benzene. Transferability between these limits is essential for a successful modeling of amorphous carbons, which are believed to contain 2D graphitic islands of varying sizes.[10,23] The calculations in Sec. II show that Kirkwood and Keating parametrizations for 2D graphite lead to large errors in benzene, including an incorrect ordering of the normal modes. The failure of these models is attributed in large part to the neglect of π-electron polarizability.[1] A simple model of this effect[1,4] is examined in Sec. II which corrects the qualitative errors in the calculated in-plane C-C vibrations in benzene. This example suggests an even larger role for quantum-mechanical effects in graphite and other sp^2 carbons with smaller π-electron band gaps.

The full tight-binding formalism for 2D graphite is described in Sec. III. The parametrization and results are given in Sec. IV. The main conclusions of this study are that (1) long-range π-electron interactions are important for the in-plane vibrations of 2D graphite, and (2) the tight-binding total-energy method is less successful here than in sp^3 bonded systems. The significance of these results is discussed in Sec. V. Some formal details are given in the appendix.

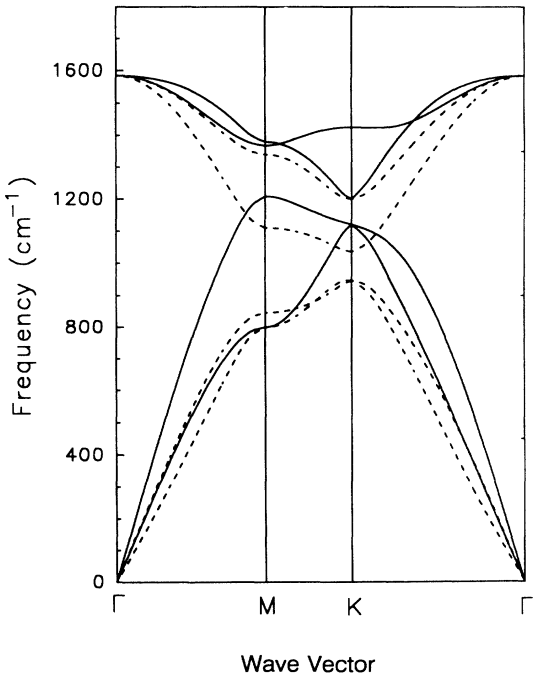

FIG. 2. Dispersion curves for the in-plane vibrations in 2D graphite calculated using the Keating (solid) and Kirkwood (dashed) models with the parameters of Table I.

TABLE I. Valence force parameters and comparison to experiment (Refs. 12, 25, and 26) of predicted in-plane elastic constants for graphite and in-plane C-C vibrational frequencies for benzene. The final entry for benzene is the rms average of the six modes.

Force constants	Kirkwood (mdyn/Å)	Keating (mdyn/Å)	Expt.
"Stretch"	$k_r=2.527$	$k_s=4.409$	
"Bend"	$k_\theta=0.565$	$k_b=0.754$	
Graphite	(Mbar)	(Mbar)	(Mbar)
c_{11}	4.7	9.6	10.6
c_{66}	2.5	4.5	4.4
Benzene	(cm^{-1})	(cm^{-1})	(cm^{-1})
E_{2g}	512	585	606
A_{2g}	575	822	922
B_{1u}	942	942	1010
B_{2u}	996	1315	1311
E_{1u}	779	921	1480
E_{2g}	1058	1222	1585
$\langle\omega^2\rangle^{1/2}$	829	981	1241

in-plane vibrations in 2D graphite. Both models were constrained to give a zone-center optic mode frequency of 1585 cm^{-1} and a SH mode at M of 800 cm^{-1}. The SH(M) mode is a pure bending motion whose frequency in these models is determined entirely by the parameters k_θ and k_b. The Kirkwood and Keating parameters used in Fig. 2 are listed in Table I along with the predicted and experimental[12] in-plane elastic constants for graphite [c_{11} and $c_{66}=(c_{11}-c_{12})/2$]. Explicit relationships between these parameters and the tensor force constants that will be introduced in Secs. III and IV of this paper are given in Table II. The Keating model reproduces the experimental elastic constants very well, while the Kirkwood model underestimates both c_{11} and c_{66} by about a factor of 2. This difference between the two models is also reflected in the different low-frequency slopes in Fig. 2. A comparison of Figs. 1 and 2 shows that the Keating model provides a reasonable fit at all frequencies, while the Kirkwood model is highly inaccurate [e.g., the LA(M) mode is off by over 400 cm^{-1}]. Neither model reproduces the initial upward curvature of the LO branch away from Γ that is seen in both the experimental data and the AD model. Equations (1) and (2) also ignore the out-of plane branches in Fig. 1, which may be modeled within a valence force approach by the addition of a four-body "puckering" interaction.[24]

TABLE II. Relationship between tensor force constants for 2D graphite in the notation of Sec. IV and Kirkwood and Keating valence force parameters.

	Kirkwood	Keating
$\phi_{xx}(0,1)$	$-k_r$	$-k_s+k_b$
$\phi_{yy}(0,1)$	$-6k_\theta$	$-3k_b$
$\phi_{xx}(0,2)$	$3k_\theta/4$	$k_b/4$
$\phi_{xy}(0,2)=-\phi_{yx}(0,2)$	$-\sqrt{3}k_\theta/4$	$-\sqrt{3}k_b/4$
$\phi_{yy}(0,2)$	$-k_\theta/4$	$-3k_b/4$

The predictions of these same Kirkwood and Keating models for the in-plane C-C vibrations of a single benzene ring are given at the bottom of Table I. For simplicity, these results were obtained by assuming that each C-H unit in benzene (C_6H_6) acts as a single entity with a mass of 13 amu.[2] The calculated frequencies are compared in Table I to the observed frequencies[25,26] for benzene modes in which the bonded C and H atoms move in phase. Some quantitative disagreement is expected here in view of the neglect of interactions with out-of-phase modes. The actual discrepancies, however, are too large to be explained by this approximation. The Keating and Kirkwood models underestimate the rms value of the experimental frequencies by over 20% and over 30%, respectively. These errors are also too large to be attributed to changes in force constants resulting from the small reduction in C-C bond length from graphite (1.42 Å) to benzene (1.39 Å).[4] The two valence force models do not even give a correct ordering of the benzene modes. It is clear from this example that the transferability of a given valence force model for sp^2 carbon must not be taken for granted.

The basic problem is that valence force models ignore the nonlocal character of π bonding. In benzene, the π electrons are delocalized around a single sixfold ring, whereas in graphite, they are delocalized over an entire 2D layer. Bonding and antibonding π states are thus well separated in benzene ($\sim$6 eV) while the corresponding bandgap for an isolated 2D graphitic layer vanishes at certain points in **k** space (cf., Sec. IV). It would be remarkable if such a large difference in electronic structure had no effect on the interactions between atoms. The transferability of any classical potential for sp^2 carbon is thus equally suspect.[27] Note that the case of sp^3 bonding differs in that the relevant electronic states are effectively

localized and there is less sensitivity to the extended environment. As long as the local coordination remains close to tetrahedral, the transferability of valence force parameters for sp^3 bonded solids does not appear to be an issue.[22]

Before abandoning a valence force description completely, it is instructive to consider a hybrid approach for sp^2 carbon in which a Kirkwood or Keating model is retained for the σ bonds while the π electrons are treated quantum mechanically. This approach of Coulson and Longuet-Higgins[1] has recently been applied extensively to polyene chains.[2–5,28] The π electrons are conveniently described by the simple tight-binding (Hückel) Hamiltonian,

$$H=-\sum_{\langle ij\rangle}[t_{ij}(|i\rangle\langle j|+|j\rangle\langle i|)+\Gamma(|\mathbf{x}_{ij}|-d_0)]\ , \tag{3}$$

where $|i\rangle$ represents a π orbital on site i and

$$t_{ij}=t_0-\alpha(|\mathbf{x}_{ij}|-d_0) \tag{4}$$

is the hopping integral between nearest-neighbor sites i and j. The second term in Eq. (3) has no effect on vibrational frequencies but prevents the collapse of π bonds; for benzene, $\Gamma=4\alpha/3$ ensures that d_0 is the equilibrium bond length. The quantity α that appears both here and in Eq. (4) is a measure of the electron-phonon interaction.[28] It is this interaction, of course, that couples the π electronic structure to both static and dynamic lattice properties. Let

$$|n\rangle=\sum_i c_{in}|i\rangle \tag{5}$$

denote an electronic eigenstate with energy E_n at equilibrium. The electronic contribution to the dynamical matrix, $\delta D_{\alpha,\beta}(r,s)$, which is the second derivative of the total electronic energy with respect to the displacements $u_{r\alpha}$ and $u_{s\beta}$ (the first and second indices represent the site and direction, respectively), is then[1]

$$\delta D_{\alpha\beta}(r,s)=2\alpha^2\sum_{\langle ij\rangle}\sum_{\langle kl\rangle}\pi_{ij,kl}\frac{\partial|\mathbf{x}_{ij}|}{\partial u_{r\alpha}}\frac{\partial|\mathbf{x}_{kl}|}{\partial u_{s\beta}}\ , \tag{6}$$

where

$$\pi_{ij,kl}=2\sum_{n\ \mathrm{occ}}\sum_{m\ \mathrm{unocc}}\frac{(c_{in}c_{jm}+c_{im}c_{jn})(c_{kn}c_{lm}+c_{km}c_{ln})}{E_n-E_m} \tag{7}$$

is the "mutual polarizability" of bonds ij and kl; "occ" and "unocc" in Eq. (7) refer to occupied and unoccupied states, respectively.

The relevant mutual polarizabilities for benzene are easily calculated and are given in Ref. 1. Figure 3 shows the resulting in-plane C-C vibrational frequencies for benzene (again with a C mass of 13 amu and neglecting H) as a function of α. A Keating model was assumed here for the σ bond contribution, with the force constants $k_s=7.3$ and $k_b=1.03$ mdyn/Å taken from Mele;[4,29] t_0 was assumed to be 3 eV. The most striking aspect of the figure is the pronounced softening of the B_{2u} mode with increasing α. The displacement pattern shown for this mode indicates an oscillation between two possible bond alternations of the sixfold ring. Within a pure valence force approach ($\alpha=0$ here), the B_{2u} mode has the highest, or close to the highest, frequency of any C-C vibration. Electronic effects, however, lower the frequency of this mode dramatically since an alternating-single-double-bond structure becomes increasingly favorable with increasing α. Experimentally, the B_{2u} mode is only the third highest of the modes shown, with a frequency of 1311 cm^{-1} (cf. Table I). A qualitatively reasonable description of benzene according to Fig. 3 would thus require an α of approximately 4–6 eV/Å. This range of α is in good agreement with that claimed for the π electrons in polyacetylene.[28]

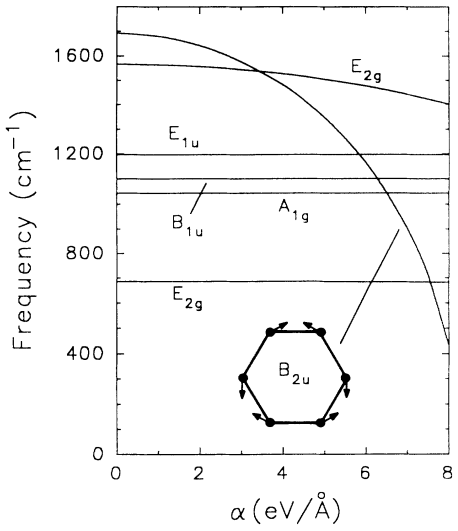

FIG. 3. In-plane C-C vibrations of a benzene ring calculated with a Keating model for σ bonds and Eqs. (3) and (4) for π electrons. The parameters used are $k_s=7.3$ mdyn/Å, $k_b=1.03$ mdyn/Å, and $t_0=3$ eV. α is the electron-phonon interaction. The inset shows the displacement pattern for the B_{2u} mode.

The energy denominator in Eq. (7) implies that electronic effects should be even more important in systems with a smaller band gap than benzene. Of particular interest for an understanding of amorphous carbons are the trends as a function of cluster size from benzene to 2D graphite. Robertson and O'Reilly showed that the bandgap in the most compact of such clusters decreases an $N^{-1/2}$, where N is the number of fused sixfold rings.[10,30] It can be seen from Fig. 1 and Table I that the highest C-C vibrational frequency is roughly the same ($\sim$1600 cm^{-1}) in the limiting cases of benzene and graphite. Simple valence force models, on the other

hand, predict that the modes in graphite extend to higher frequencies because of the larger number of C neighbors (cf. Fig. 2 and Table I). The observed near equivalence of the upper cutoffs in benzene and graphite is thus most likely a coincidence that results from a cancellation between this coordination effect and a greater softening of the graphite modes due to a larger π-electron polarizability. Calculations based on the hybrid approach just presented are suggestive of such a cancellation, but the resulting description of graphite is quite poor.[31] It is thus of interest to consider a fully quantum-mechanical treatment of 2D graphite in which no approximations are made *a priori* about the form of the σ interactions.

III. FULL TIGHT-BINDING FORMALISM FOR 2D GRAPHITE

The full tight-binding total energy method for phonons is described in detail in Ref. 17. The present section summarizes the essential features of this formalism and outlines the separation between σ and π contributions in 2D graphite.

The fundamental ansatz of this method is that the total energy of a solid may be divided as

$$E_{\rm tot}=E_{\rm BS}+E_{\rm rep} , \tag{8}$$

where $E_{\rm BS}$ is the electronic band-structure energy and $E_{\rm rep}$ is an empirical interatomic repulsion.[13] $E_{\rm BS}$ is the sum of the energies of the occupied one-electron states which result from an empirical tight-binding Hamiltonian, H. $E_{\rm rep}$ corrects for the double counting of electron-electron interactions in $E_{\rm BS}$ and for additional contributions to the total energy, such as the Coulomb interaction between ions. Here, as in most previous work, $E_{\rm rep}$ is assumed to be describable in terms of a nearest-neighbor pair potential.[13–17] Phonon states are then affected only by the coefficients of the harmonic expansion,

$$E_{\rm rep}=\sum_{\langle ij\rangle}(U_1\epsilon_{ij}+U_2\epsilon_{ij}^2) , \tag{9}$$

where $\epsilon_{ij}=(d_{ij}-d_0)/d_0$ is the fractional change in the ijth bond length relative to the equilibrium spacing, d_0. The choice of parameters, U_1 and U_2, is discussed in Sec. IV.

Electronic eigenstates are constructed from an orthonormal set of atomiclike basis functions with symmetries s, p_x, p_y, and p_z at each site. For 2D graphite lying perpendicular to the z axis, the first three of these functions form sp^2 (σ) hybrid orbitals, while the p_z functions represent the π electrons. Within the empirical tight-binding method, only the matrix elements of H and their dependences on atomic coordinates need to be specified explicitly.[32,33] The present work assumes that (1) interatomic interactions are restricted to first-nearest neighbors, (2) only two-center integrals[32] contribute to the matrix elements of H, and (3) the two-center parameters ($V_{ss\sigma}$, $V_{sp\sigma}$, $V_{pp\sigma}$, and $V_{pp\pi}$) scale as d^{-2}, where d is the bond length. This leaves only six empirical parameters (the four V's plus the on-site s- and p-level energies), which are required to reproduce the band structure of 2D graphite. The procedure for constructing the 8×8 **k**-space Hamiltonian matrix from these parameters is well known;[32,33] the general form of the 4×4 nearest-neighbor hopping matrix is reviewed in the Appendix.

The atomic force constants of interest for lattice dynamics are given by

$$\phi_{\alpha\beta}(l\nu;l'\nu')=\frac{\partial^2E_{\rm tot}}{\partial u_\alpha(l\nu)\partial u_\beta(l'\nu')} , \tag{10}$$

where $u_\alpha(l,\nu)$ is the displacement of the atom on sublattice ν in the lth unit cell in the direction α. The contribution from $E_{\rm BS}$ in Eq. (8) may be expressed in terms of the unperturbed electronic Green's function,

$$G_0(E)=(E+i0^+-H)^{-1} , \tag{11}$$

yielding[17]

$$\phi_{\alpha\beta}(l,\nu;l',\nu')=\phi_{\alpha\beta}^{\rm BS,SR}(l,\nu;l',\nu')+\phi_{\alpha\beta}^{\rm BS,LR}(l,\nu;l',\nu')+\frac{\partial^2E_{\rm rep}}{\partial u_\alpha(l,\nu)\partial u_\beta(l',\nu')} , \tag{12}$$

where

$$\phi_{\alpha\beta}^{\rm BS,SR}(l,\nu;l',\nu')=-\frac{2}{\pi}\int_{-\infty}^{E_F}{\rm Im\,Tr}\left[G_0(E)\frac{\partial^2H}{\partial u_\alpha(l,\nu)\partial u_\beta(l',\nu')}\right]dE \tag{13}$$

and

$$\phi_{\alpha\beta}^{\rm BS,LR}(l,\nu;l',\nu')=-\frac{2}{\pi}\int_{-\infty}^{E_F}{\rm Im\,Tr}\left[G_0(E)\frac{\partial H}{\partial u_\alpha(l,\nu)}G_0(E)\frac{\partial H}{\partial u_\beta(l',\nu')}\right]dE . \tag{14}$$

[The factors of 2 in Eqs. (13) and (14) are for spin; the traces are computed for a single spin orientation.] Equation (13) is a short-ranged (SR) interaction since the second derivative vanishes unless the sites l,ν and l',ν' are directly coupled by H (i.e., are nearest neighbors). Equation (14), on the other hand, represents a potentially long-ranged (LR) contribution whose decay is determined by that of the bulk Green's function. The traces in Eqs. (13) and (14) may be evaluated in either real or reciprocal space. The latter choice has been shown previously to clarify the connection between the LR term and the electronic polarizability.[17] For the simple π-electron model of Eqs. (3) and (4), Eq. (14) reduces to Eq. (6). In general, the required derivatives in Eqs. (13) and (14) are easily

calculated analytically. Results for the first derivatives of H, which are essential for what follows, are given in the Appendix.

By symmetry, all force constants of the form ϕ_{xz}, ϕ_{yz}, ϕ_{zx}, and ϕ_{zy} are strictly zero for 2D graphite. Also by symmetry, the unperturbed Green's function $G_0(E)$ does not couple σ and π orbitals. The trace in Eq. (13) may thus be expanded schematically as

$$\mathrm{Tr}[GH'']=\mathrm{Tr}[G_\sigma H''_{\sigma\sigma}]+\mathrm{Tr}[G_\pi H''_{\pi\pi}] , \tag{15}$$

which allows the separation of σ and π contributions to $\phi^{\mathrm{BS,SR}}$ for both in-plane and out-of-plane displacements. The situation is more complicated for $\phi^{\mathrm{BS,LR}}$. It is shown in the Appendix that $\partial H/\partial u_\alpha(lv)$ does not couple σ and π orbitals for $\alpha=x$ or y; the trace in Eq. (14) is thus also separable into σ and π contributions for in-plane displacements:

$$\mathrm{Tr}[GH'GH']_{\text{in-plane}}=\mathrm{Tr}[G_\sigma H'_{\sigma\sigma}G_\sigma H'_{\sigma\sigma}] + \mathrm{Tr}[G_\pi H'_{\pi\pi}G_\pi H'_{\pi\pi}] . \tag{16}$$

The derivative $\partial H/\partial u_z(lv)$, on the other hand, couples only dissimilar orbitals; the resulting mixing of σ and π contributions,

$$\mathrm{Tr}[GH'GH']_{\text{out-of-plane}}=\mathrm{Tr}[G_\sigma H'_{\sigma\pi}G_\pi H'_{\pi\sigma} + G_\pi H'_{\pi\sigma}G_\sigma H'_{\sigma\pi}] , \tag{17}$$

is a consequence of the rehybridization that occurs at each carbon site during out-of-plane motion.

IV. PARAMETRIZATION AND RESULTS

Several tight-binding parametrizations for carbon have been reported in the literature.[34–37] The most suitable for the present purposes is that of Tománek and Louie,[36] which has recently been used in a tight-binding total-energy study of carbon clusters.[38] The diagonal s- and p-level energies in this parametrization are $E_s=-7.3$ eV and $E_p=0.0$ eV, respectively. At the graphite equilibrium spacing, the off-diagonal, two-center parameters are $V_{ss\sigma}=-4.30$ eV, $V_{sp\sigma}=4.98$ eV, $V_{pp\sigma}=6.38$ eV, and $V_{pp\pi}=-2.66$ eV. These values were all determined from a global fit to density-functional theory predictions for carbon dimers, 2D graphite and diamond over a range of nearest-neighbor distances.[38] A d^{-2} scaling of off-diagonal parameters was built directly into the parametrization.

The resulting energy band structure for 2D graphite at equilibrium consists of bonding and antibonding σ bands separated by over 10 eV and bonding and antibonding π bands that are degenerate at the K point. These degenerate states lie at the Fermi level (E_F) and are split in real graphite by interlayer interactions. Larger-scale features of the tight-binding bands are in reasonable agreement with experimental results for graphite.[10,30] The main discrepancies lie in the antibonding bands, which are too narrow in the tight-binding model. This is particularly apparent for the antibonding π band; experimentally, this band is broader than the bonding π band but, with only nearest-neighbor tight-binding interactions, the two π bands are symmetric about E_F.

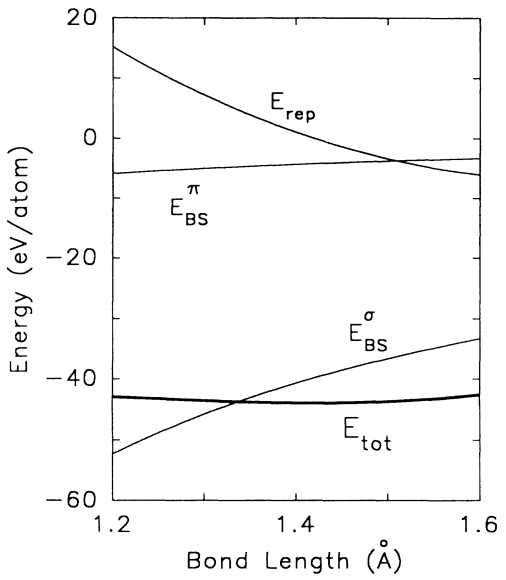

FIG. 4. Tight-binding total energy and its various contributions for 2D graphite as a function of the nearest-neighbor bond length. E^σ_{BS}, E^π_{BS} and E_{rep} are the σ and π band-structure energies and the repulsive energy, respectively.

Band-structure contributions to the total energy were calculated separately for σ and π electrons for a range of nearest-neighbor bond lengths. These, and all other Brillouin-zone integrations in this paper, were performed using a set of 45 special **k** points in the irreducible Brillouin zone.[39] The results for E^σ_{BS} and E^π_{BS} are shown in Fig. 4 along with the empirically determined repulsive

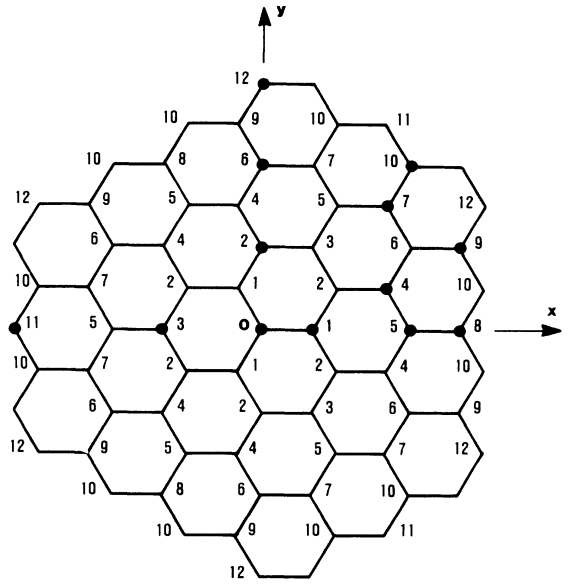

FIG. 5. Portion of 2D graphite lattice with x and y axes defined and first 12 nearest-neighbor shells about the origin (site 0) labeled.

TABLE III. Nearest-neighbor information corresponding to Fig. 6 for an A sublattice site at the origin. The first four columns give the shell number, the sublattice on which the shell lies (A or B), the number of neighbors in the shell, and the distance from the origin, respectively. The last column gives the coordinates of the reference sites for which force constants were calculated directly. The last two columns are in units of the nearest-neighbor distance.

Shell no.	Sublattice	No. in shell	Distance	Reference site
1	B	3	1	(1,0)
2	A	6	$\sqrt{3}$	$(0,\sqrt{3})$
3	B	3	2	(−2,0)
4	B	6	$\sqrt{7}$	$(5/2,\sqrt{3}/2)$
5	A	6	3	(3,0)
6	A	6	$2\sqrt{3}$	$(0,2\sqrt{3})$
7	B	6	$\sqrt{13}$	$(5/2,3\sqrt{3}/2)$
8	B	3	4	(4,0)
9	B	6	$\sqrt{19}$	$(4,\sqrt{3})$
10	A	12	$\sqrt{21}$	$(3,2\sqrt{3})$
11	B	3	5	(−5,0)
12	A	6	$3\sqrt{3}$	$(0,3\sqrt{3})$

energy and the total energy. The coefficients U_1 and U_2 in Eq. (9) were constrained to give an equilibrium spacing of 1.42 Å and an upward curvature in $E_{\rm tot}$ at equilibrium that reproduces the in-plane area modulus, $c_{11}+c_{12}$, in crystalline graphite. The fitted values are $U_1=-46.806$ eV and $U_2=119.105$ eV. Figure 4 shows that $E_{\rm rep}$ mainly balances the strong attraction of the σ electrons, although the π-electron attraction is also important. Unlike some tight-binding total-energy calculations[36] in which the entire range of the curves in Fig. 4 is relevant (or even a wider range[40]), the present lattice dynamical study is influenced only by the first and second derivatives of these curves at equilibrium.

Once the tight-binding parameters and U_1 and U_2 are specified, it is straightforward, albeit tedious, to calculate the atomic force constants. Figure 5 shows a portion of the 2D graphite lattice and coordinate axes used for reference. The labels represent the nearest-neighbor shell number of a given site relative to the origin (0). For each shell, it is sufficient to calculate the atomic force constants between the origin and one member of the shell; the corresponding force constants for other members of the shell may then be obtained by group theory. The solid dots in Fig. 5 indicate the particular sites chosen to represent their shells. The coordinates of these sites and other information on the first 12 nearest-neighbor shells is given in Table III. In what follows, the simplified notation $\phi_{\alpha\beta}(0,N)$ will be used to denote the force constants between the origin and the representative site in the Nth neighbor shell. Although suppressed here, the sublattice information in Table III is important, of course, for constructing the dynamical matrix.[41]

TABLE IV. Contributions to the nearest-neighbor force constants (in eV/Å^2) from the repulsive pair potential and the σ and π short-ranged band-structure terms.

	Rep.	σ,SR	π,SR
$\phi_{xx}(0,1)$	−118.136	61.328	8.309
$\phi_{yy}(0,1)$	23.213	−38.850	−2.770
$\phi_{zz}(0,1)$	23.213	−36.341	−12.182

Both the repulsive pair potential and the SR term in Eq. (12) contribute only to the nearest-neighbor force constants, $\phi_{\alpha\beta}(0,1)$, which are diagonal by symmetry. The repulsive contribution is easily calculated analytically[17] and the results are given in the first column of Table IV. The remaining two columns give the σ and π SR band-structure contributions, respectively, as separated in Eq. (15). The traces in Eq. (15) are evaluated in real space, as are those in Eqs. (16) and (17) which are needed for the LR terms below. In both the SR and LR calculations, the integrand is first evaluated off the real energy axis and then analytically continued back to this axis before performing the integration.[42] This procedure ensures rapid convergence in the number of $\mathbf{k}$ points used to evaluate the required Green's-function matrix elements. These matrix elements were evaluated in terms of the σ and π eigenstates at the above-mentioned set of 45 special $\mathbf{k}$ points in the irreducible Brillouin zone and equivalent larger sets in cases of lower symmetry.

The LR term is more complicated to evaluate because of the many paths that contribute to the trace in Eq. (14) in a real-space approach.[17] Group theory is again helpful for restricting the number of Green's-function matrix elements that need to be calculated for a given nearest-neighbor shell. The required range of the Green's function is longer than that of the force constant being calculated. For example, even in the simple case of $\phi_{\alpha\beta}(0,1)$, the trace in Eq. (14) involves Green's-function matrix elements out to the fourth-nearest neighbor.

The calculated σ contributions to the in-plane LR force constants for the first 12 nearest neighbors are listed in Table V. Blank entries are zero by symmetry. (This was confirmed numerically in each case as a test of the computer code.) The last two columns in Table V give information relevant to the range of force constants derived from σ electrons. Mazur and Pollmann[17] suggested

TABLE V. Contributions to the near-neighbor, in-plane force constants (in eV/Å^2) from the σ long-ranged band-structure term. $\Sigma_{xx}(N)$ is the partial sum of the right-hand side of Eq. (18) (xx component) out to shell N. The value in parentheses at the bottom of this column is the directly calculated value of $\phi_{xx}(0,0)$. The last column gives the deviation of $\Sigma_{xx}(N)$ from this value (in %).

N	$\phi_{xx}(0,N)$	$\phi_{xy}(0,N)$	$\phi_{yx}(0,N)$	$\phi_{yy}(0,N)$	$\Sigma_{xx}(N)$	Deviation
1	6.271			8.724	22.493	+0.8
2	1.827	−0.907	0.907	−1.758	22.700	+1.7
3	0.510			−0.318	22.988	+3.0
4	0.149	0.631	0.631	−0.417	22.184	−0.6
5	−0.041			0.061	22.244	−0.3
6	0.067	−0.031	0.031	−0.028	22.361	+0.2
7	−0.002	0.013	0.013	0.001	22.358	+0.2
8	0.005			−0.015	22.343	+0.1
9	0.004	0.003	0.003	−0.018	22.301	−0.6
10	−0.001	0.002	−0.005	−0.003	22.277	−0.2
11	0.000			−0.003	22.272	−0.2
12	−0.005	−0.004	0.004	−0.009	22.230	−0.4
					(22.313)	

this convergence test based on the relationship

$$\phi_{\alpha\beta}(0;0) = -\sum_{l\nu\neq 0} \phi_{\alpha\beta}(0;l,\nu) \ . \tag{18}$$

The sixth column in Table V gives the contribution to the right-hand side of Eq. (18) from the σ contributions to $\phi_{xx}^{\mathrm{SB,LR}}(0;l,\nu)$ for the first N nearest-neighbor shells. The value in parentheses at the bottom of the column is the calculated result for $\phi_{xx}^{\mathrm{BS,LR}}(0;0)$ based on Eq. (14). The last column in the table shows how well the partial sum agrees with this value. [Note that when constructing the dynamical matrix, $\phi_{\alpha\beta}(0;0)$ is obtained from the sum in Eq. (18) out to the range at which the force constants are truncated.] Convergence to within 1% is already achieved by the fourth-nearest-neighbor shell and is not improved substantially by the inclusion of more distant neighbors. This is similar to the range of σ interactions found by Mazur and Pollmann[17] for diamond-structure Si.

Table VI gives the corresponding results for the π contributions to the in-plane LR force constants. The convergence is much slower than for the σ contributions. Inclusion of the first six nearest-neighbor shells is required for even 5% convergence and 1% convergence is not even achieved by the 12th shell. The magnitudes and signs of the errors exhibit no clear pattern as more neighbors are included. The results in Table VI confirm the existence of long-ranged interactions in 2D graphite due to π-electron delocalization. The in-plane vibrations in graphite are thus clearly affected by nearly metallic π bonding as well as covalent σ bonding.

Table VII lists the remaining LR force constants that give rise to out-of-plane vibrations that mix σ and π electrons [cf. Eq. (17)]. The convergence here is similar to that for the pure-σ, in-plane interactions in Table V.

The dynamical matrix[41] was constructed from the force constants in Tables IV–VII out to the 12th nearest neighbor. Longer-ranged, in-plane π interactions may still contribute at the 2% level, but are unlikely to change things significantly. The resulting tight-binding phonon spectrum for 2D graphite is shown in Fig. 6 along with the experimental data[20] from Fig. 1. The tight-binding results are clearly inferior to those of the AD model.[18] Along Γ-M, the two highest branches in Fig. 6 are too high by 15%, the ZO branch is too low by 20%, and the

TABLE VI. Contributions to the near-neighbor, in-plane force constants (in eV/Å^2) from the π long-ranged band-structure term. The setup is the same as in Table V.

N	$\phi_{xx}(0,N)$	$\phi_{xy}(0,N)$	$\phi_{yx}(0,N)$	$\phi_{yy}(0,N)$	$\Sigma_{xx}(N)$	Deviation
1	5.752			−0.525	7.841	+24.7
2	0.867	1.078	−1.078	−1.118	6.878	+9.4
3	0.508			−1.157	5.904	−6.1
4	0.339	−0.121	−0.121	0.006	6.939	+10.4
5	−0.388			−0.061	5.742	−8.7
6	0.113	−0.002	0.002	−0.007	6.060	−3.6
7	0.096	0.094	0.094	−0.066	6.150	−2.2
8	0.252			−0.047	6.458	+2.7
9	−0.024	0.049	0.049	0.008	6.410	+1.9
10	−0.018	−0.108	0.009	0.010	6.362	+1.2
11	0.058			−0.082	6.326	+0.6
12	−0.013	−0.003	0.003	−0.044	6.155	−2.1
					(6.287)	

TABLE VII. Contributions to the near-neighbor, out-of-plane force constants (in eV/Å^2) from the long-ranged band-structure term. The setup of the last two columns is the same as in Tables V and VI but for the zz component.

N	$\phi_{zz}(0,N)$	$\Sigma_{zz}(N)$	Deviation
1	21.183	63.549	−3.0
2	0.088	64.077	−2.2
3	−0.371	62.964	−3.9
4	0.534	66.168	+1.0
5	−0.090	65.628	+0.2
6	0.017	65.730	+0.4
7	0.008	65.778	+0.4
8	−0.073	65.559	+0.1
9	−0.026	65.403	−0.1
10	0.001	65.415	−0.1
11	−0.065	65.220	−0.4
12	0.016	65.316	−0.3
		(65.494)	

lower SH branch is too low by as much as 30%, compared to experiment. The tight-binding predictions near K are likely to be even less reliable given their larger deviation there from the AD model.

The overestimate of the phonon bandwidth in Fig. 6 appears to be a general feature of tight-binding calculations in which the repulsive pair potential is fit to the bulk modulus[17,43] (or its equivalent here, $c_{11}+c_{12}$). The value of U_2 may be adjusted to give the proper bandwidth at the expense of a poorer description of elastic properties.[17] This will not be shown here since it simply lowers all of the high-frequency branches without changing anything qualitatively.

One additional feature of the tight-binding results that deserves comment is the slight upward curvature of the highest-frequency branch in Fig. 6 along Γ-M and Γ-K. This behavior, which is also seen in the AD model and the experimental results, is impossible to describe within the Kirkwood or Keating models. A similar upward curvature at Γ is predicted by tight-binding phonon calculations for polyacetylene.[3]

The tight-binding predictions for the LO(Γ) and ZO(Γ) modes were checked by independent frozen-phonon calculations. This approach is computationally much simpler than the calculation of atomic force constants, but is useful only at high-symmetry points.[6,44] For each of the two modes, the total energy was calculated directly from Eq. (8) as a function of the amplitude of the phonon distortion. The results are plotted in Fig. 7 along with various contributions to the total energy; u represents either the in-plane (top) or out-of-plane (bottom) displacement of the two sublattices. The mode frequencies are easily extracted from the curvatures of the ΔE vs u curves. This yields 1789 and 696 cm^{-1} for LO(Γ) and ZO(Γ), respectively, in excellent agreement with Fig. 6.

Figure 7 also shows that the band-structure and repulsive contributions to the total energy behave in opposite manners for the in-plane and out-of-plane modes. For the LO(Γ) distortion, both the σ and π band-structure energies are destabilizing and the restoring force is provided by the repulsive potential. For the ZO(Γ) distortion, on the other hand, the band-structure energy provides the restoring force because of the energy increase

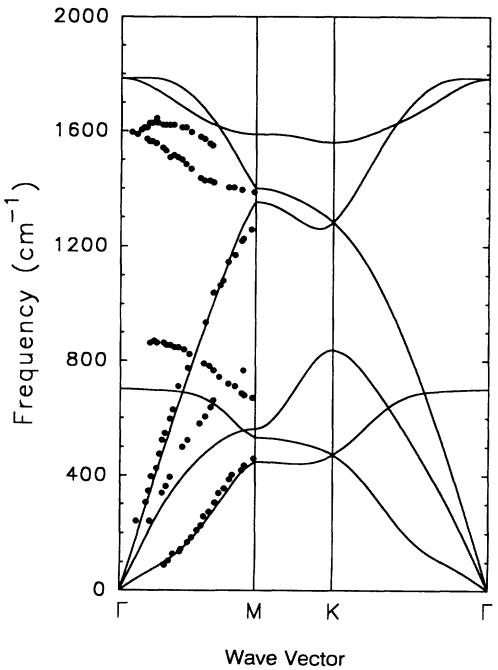

FIG. 6. Phonon dispersion curves for 2D graphite calculated from tight-binding force constants in Table IV–VII. The dots are experimental data from Ref. 20.

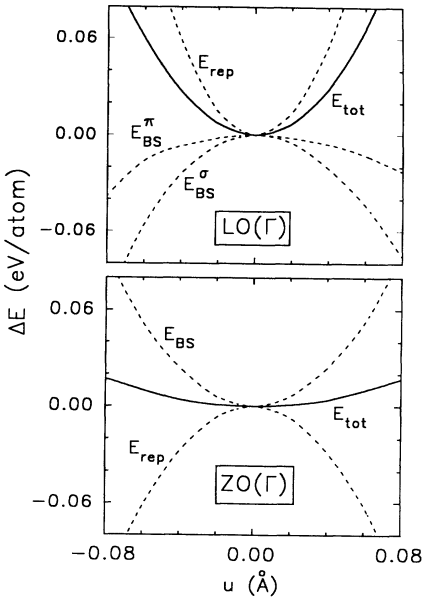

FIG. 7. Tight-binding results for the change in total energy and its various contributions as a function of the relative displacement between the two sublattices (u) for the in-plane LO(Γ) and out-of-plane ZO(Γ) modes.

associated with σ-π mixing. The repulsive contribution to ZO(Γ) is destabilizing because all nearest-neighbor bonds are stretched. The out-of-plane motion (perpendicular to the bonds) in this case is affected only by the U_1 parameter in Eq. (9). The suggested adjustment of U_2 above to reduce the phonon bandwidth in Fig. 6 would thus leave the ZO(Γ) frequency unchanged.

V. DISCUSSION

In general, the present tight-binding description of the lattice dynamics of 2D graphite is much less successful than previous applications of this approach to sp^3-bonded solids.[15–17] There is no obvious reason why this should be so since the quality of the parametrized electronic band structure in each case is comparable. The problem may be fundamental in nature or it may be an artifact of the chosen parametrization. One can certainly question whether a nearest-neighbor hopping model is sufficient here for the π electrons since it is known that a second-neighbor interaction is required to describe the asymmetry between the π and π^* bands.[10,30] Other generalizations that might improve matters include using a different nearest-neighbor $V_{pp\pi}$ interaction for σ and π electrons,[35] a different E_p value in the two cases, or a scaling law other than d^{-2}. Some preliminary tests were made of all of these effects, but none seemed particularly promising.

On a more fundamental level, the problem may have to do with an inadequate treatment of electron-electron interactions. The addition of Coulomb interactions to the tight-binding Hamiltonian, for example, would alter the resulting force constants due to screening effects.[16] Whether such interactions are important in 2D graphite is unclear. On the one hand, Coulomb effects do tend to be more pronounced in lower dimensional systems. On the other, the importance of Coulomb interactions even in one-dimensional conducting polymers is still highly controversial.[28]

It may simply be that an accurate, simultaneous description of both delocalized, nearly metallic π bonding and localized, covalent σ bonding is too much to ask of a semiempirical approach. Springborg[45] has argued that, because of subtleties in the electron-electron interaction, it may not be formally possible to divide the total energy up into σ and π contributions, as was essentially done here for in-plane vibrations. Both Figs. 4 and 7 show that the behavior of the total energy in the tight-binding approach results from a near cancellation of competing effects. Since these individual effects themselves behave differently for different phonon modes (Fig. 7), it is perhaps remarkable that the tight-bonding approach does as well as it does. After all, Fig. 6 does get the much-different bandwidths of in-plane and out-of-plane modes correct to within 20%, despite the much different physics involved. The greater success of the tight-binding approach in sp^3-bonded solids may not be a fair comparison, given that valence force models are also more successful in that case.

One may conclude from the present study that the modeling of the vibrational properties of π-bonded solids is much more difficult than has been generally appreciated. Long-range π-electron interactions are clearly important in graphite as well as polyene chains.[2–5] Such interactions are highly nonlocal, which makes the transferability of any simple approach highly questionable. Unfortunately, the present tight-binding study has done more to identify these problems than to solve them. It is hoped that this work will stimulate further discussion of these issues and new ideas on how to proceed.[46] Progress in this area would be particularly valuable for modeling the vibrational properties of amorphous carbons and fullerenes.

APPENDIX: NEAREST-NEIGHBOR HOPPING MATRIX AND ITS DERIVATIVE

Let $H_{ij}(\tau,\tau')$ be the 4×4 matrix block of the tight-binding Hamiltonian that couples τ orbitals on site i with τ' orbitals on nearest-neighbor site j. If (l_x,l_y,l_z) are the direction cosines from i to j, then[32,33]

$$H_{ij}(s,s)=v_{ss\sigma} ,$$

$$H_{ij}(s,p_x)=-H_{ij}(p_x,s)=l_x V_{sp\sigma} ,$$

$$H_{ij}(s,p_y)=-H_{ij}(p_y,s)=l_y V_{sp\sigma} ,$$

$$H_{ij}(s,p_z)=-H_{ij}(p_z,s)=l_z V_{sp\sigma} ,$$

$$H_{ij}(p_x,p_x)=l_x^2 V_{pp\sigma}+(1-l_x^2)V_{pp\pi} ,$$

$$H_{ij}(p_y,p_y)=l_y^2 V_{pp\sigma}+(1-l_y^2)V_{pp\pi} ,$$

$$H_{ij}(p_z,p_z)=l_z^2 V_{pp\sigma}+(1-l_z^2)V_{pp\pi} ,$$

$$H_{ij}(p_x,p_y)=H_{ij}(p_y,p_x)=l_x l_y(V_{pp\sigma}-V_{pp\pi}) ,$$

$$H_{ij}(p_x,p_z)=H_{ij}(p_z,p_x)=l_x l_z(V_{pp\sigma}-V_{pp\pi}) ,$$

$$H_{ij}(p_y,p_z)=H_{ij}(p_z,p_y)=l_y l_z(V_{pp\sigma}-V_{pp\pi}) .$$

Recall that the σ orbitals are s, p_x, and p_y and the π orbital is p_z.

Equations (13) and (14) in the text require the first and second derivatives of the Hamiltonian, which are most conveniently evaluated in real space. The result will simply be stated here for the first derivative of the H_{ij} block defined above. Let

$$H'_\alpha \equiv \frac{\partial H_{ij}}{\partial u_{j\alpha}} = -\frac{\partial H_{ij}}{\partial u_{i\alpha}} .$$

The matrix elements of H'_α are

$$H'_\alpha(s,s)=-2l_\alpha(V_{ss\sigma}/d_0)\ ,$$

$$H'_\alpha(s,p_x)=-H'_\alpha(p_x,s)=(\delta_{x\alpha}-3l_xl_\alpha)(V_{sp\sigma}/d_0)\ ,$$

$$H'_\alpha(s,p_y)=-H'_\alpha(p_y,s)=(\delta_{y\alpha}-3l_yl_\alpha)(V_{sp\sigma}/d_0)\ ,$$

$$H'_\alpha(s,p_z)=-H'_\alpha(p_z,s)=\delta_{z\alpha}(V_{sp\sigma}/d_0)\ ,$$

$$H'_\alpha(p_x,p_x)=2l_x(\delta_{x\alpha}-2l_xl_\alpha)(V_{pp\sigma}/d_0)-2(l_\alpha-2l_x^2l_\alpha+\delta_{x\alpha}l_x)(V_{pp\pi}/d_0)\ ,$$

$$H'_\alpha(p_y,p_y)=2l_y(\delta_{y\alpha}-2l_yl_\alpha)(V_{pp\sigma}/d_0)-2(l_\alpha-2l_y^2l_\alpha+\delta_{y\alpha}l_y)(V_{pp\pi}/d_0)\ ,$$

$$H'_\alpha(p_z,p_z)=-2l_\alpha(V_{pp\pi}/d_0)\ ,$$

$$H'_\alpha(p_x,p_y)=H'_\alpha(p_y,p_x)=(l_x\delta_{y\alpha}+l_y\delta_{x\alpha}-4l_xl_yl_\alpha)(V_{pp\sigma}-V_{pp\pi})/d_0\ ,$$

$$H'_\alpha(p_xp_z)=H'_\alpha(p_z,p_x)=l_x\delta_{z\alpha}(V_{pp\sigma}-V_{pp\pi})/d_0\ ,$$

$$H'_\alpha(p_y,p_z)=H'_\alpha(p_z,p_y)=l_y\delta_{z\alpha}(V_{pp\sigma}-V_{pp\pi})/d_0\ ,$$

where d_0 is the bond length and use has been made of the fact that $l_z=0$ at equilibrium. Note that only the 4th, 10th, and 11th lines here couple σ and π orbitals. For $\alpha=x$ or y, these lines vanish and there is no mixing of σ and π states. For $\alpha=z$, all lines other than these vanish and the σ-π mixing is all that remains.

[1]C. A. Coulson and H. C. Longuet-Higgins, Proc. R. Soc. London, Ser. A **191**, 38 (1947); A **193**, 456 (1948).

[2]T. Kakitani, Prog. Theor. Phys. **51**, 656 (1974).

[3]E. J. Mele and M. J. Rice, Solid State Commun. **34**, 339 (1980).

[4]E. J. Mele, Mol. Cryst. Liq. Cryst. **77**, 25 (1981).

[5]L. Piseri, R. Tubino, and G. Dellepiane, Solid State Commun. **44**, 1589 (1982).

[6]For example, C. T. Chan, K. M. Ho, and W. A. Kamitakahara, Phys. Rev. B **36**, 3499 (1987).

[7]J. G. Kirkwood, J. Chem. Phys. **7**, 506 (1939).

[8]P. N. Keating, Phys. Rev. **145**, 637 (1966).

[9]R. L. Capelletti, J. R. D. Copley, W. A. Kamitakahara, F. Li, J. S. Lannin, and D. Ramage, Phys. Rev. Lett. **66**, 3261 (1991), and references therein.

[10]J. Robertson, Adv. Phys. **35**, 317 (1986), and references therein.

[11]M. A. Tamor, J. A. Haire, C. H. Wu, and K. C. Hass, Appl. Phys. Lett. **54**, 123 (1989).

[12]See M. S. Dresselhaus and G. Dresselhaus, in *Light Scattering in Solids III,* edited by M. Cardona and G. Güntherodt, Topics in Applied Physics Vol. 51 (Springer, Berlin, 1982), p. 3, for a review of the earlier literature.

[13]D. J. Chadi, Phys. Rev. Lett. **41**, 1062 (1978).

[14]For example, M. W. Finnis, K. L. Lear, and D. G. Pettifor, Phys. Rev. Lett. **52**, 291 (1984).

[15]For example, D. H. Lee and J. D. Joannopoulos, Phys. Rev. Lett. **48**, 1846 (1982).

[16]For example, O. L. Allerhand, D. G. Allan, and E. G. Mele, Phys. Rev. Lett. **55**, 2700 (1985).

[17]A. Mazur and J. Pollmann, Phys. Rev. B **39**, 5261 (1989).

[18]R. Al-Jishi and G. Dresselhaus, Phys. Rev. B **26**, 4514 (1982).

[19]P. Lespade, R. Al-Jishi, and M.S. Dresselhaus, Carbon **20**, 427 (1982).

[20]C. Oshima, T. Aizawa, R. Souda, Y. Ishizawa, and Y. Sumiyoshi, Solid State Commun. **65**, 1601 (1988).

[21]T. Aizawa, R. Souda, S. Otani, Y. Ishizawa, and C. Oshima, Phys. Rev. B **42**, 11 469 (1990); **43**, 12 060, (1991).

[22]For example, R. Alben, D. Weaire, J. E. Smith, and M. H. Brodsky, Phys. Rev. B **11**, 2271 (1975).

[23]D. Beeman, J. Silverman, R. Lynds, and M. R. Anderson [Phys. Rev. B **30**, 870 (1984)] examined the vibrational properties of various amorphous carbon networks using a Kirkwood model.

[24]A. Yoshimori and Y. Kitano, J. Phys. Soc. Jpn. **11**, 352 (1956).

[25]R. D. Mair and D. F. Hornig, J. Chem. Phys. **17**, 1236 (1949).

[26]G. Herzberg, *Infrared and Raman Spectra of Polyatomic Molecules* (Van Nostrand, New York, 1945).

[27]For example, J. Tersoff, Phys. Rev. Lett. **61**, 2879 (1988). While this potential has not been extensively tested for vibrational properties, it is unlikely to do any better than the Kirkwood and Keating models. For 2D graphite, it predicts a zone-center optic mode of 2540 cm^{-1}, nearly 60% higher than experiment.

[28]A. J. Heeger, S. Kivelson, J. R. Schrieffer, W.-P. Su, Rev. Mod. Phys. **60**, 781 (1988).

[29]Note that the stretching force constant here is significantly larger than in Table I. For $\alpha=0$, the Mele parameters give a zone-center optic mode in 2D graphite of 1994 cm^{-1}, about 26% too large.

[30]J. Robertson and E. P. O'Reilly, Phys. Rev. B **35**, 2946 (1987).

[31]A nonzero α within this model does soften the zone-center optic mode in graphite but it also produces a much larger, unphysical, softening of one of the nondegenerate K-point modes.

[32]J. C. Slater and G. F. Koster, Phys. Rev. **94**, 1498 (1954).

[33]W. A. Harrison, *Electronic Structure and the Properties of Solids* (Freeman, San Francisco, 1980).

[34]D. J. Chadi, J. Vac. Sci. Technol. A **2**, 948 (1984).

[35]J. Robertson, Philos. Mag. **47**, L33 (1983).

[36]D. Tománek and S. G. Louie, Phys. Rev. B **37**, 8327 (1988).

[37]L. Goodwin, J. Phys.: Condens. Matter **3**, 3869 (1991).

[38]D. Tománek and M. A. Schlüter, Phys. Rev. Lett. **67**, 2331 (1991).

[39]S. L. Cunningham, Phys. Rev. B **10**, 4988 (1974).

[40]M. A. Tamor and K. C. Hass, J. Mater. Res. **5**, 2273 (1990).

[41]A. A. Maradudin, E. W. Montroll, G. H. Weiss, and I. P. Ipatova, *Theory of Lattice Dynamics in the Harmonic Approximation* (Academic, New York, 1971).

[42]K. C. Hass, B. Velický, and H. Ehrenreich, Phys. Rev. B **29**, 3697 (1984).
[43]C. H. Xu, C. Z. Wang, C. T. Chan, and K. M. Ho, Phys. Rev. B **43**, 5024 (1991).
[44]D. J. Chadi and R. M. Martin, Solid State Commun. **19**, 643 (1976).
[45]M. Springborg, Phys. Scr. **T13**, 306 (1986).
[46]D. W. Brenner, Phys. Rev. B **42**, 9458 (1990), for example, describes a classical potential for carbon that incorporates some nonlocal π-electron effects, although this potential is not intended for use in vibrational calculations.